ACS Biomaterials SCIENCE & ENGINEERING

pubs.acs.org/journal/abseba

Article

# Development and Characterization of Isogenic Cardiac Organoids from Human-Induced Pluripotent Stem Cells Under Supplement Starvation Regimen

Alejandra Patino-Guerrero, Ruben D. Ponce Wong, Vikram D. Kodibagkar, Wuqiang Zhu, Raymond Q. Migrino, Oliver Graudejus, and Mehdi Nikkhah*

Cite This: https://doi.org/10.1021/acsbiomaterials.2c01290

Read Online

ACCESS | Metrics & More | Article Recommendations | Supporting Information



**ABSTRACT:** The prevalence of cardiovascular risk factors is expected to increase the occurrence of cardiovascular diseases (CVDs) worldwide. Cardiac organoids are promising candidates for bridging the gap between *in vitro* experimentation and translational applications in drug development and cardiac repair due to their attractive features. Here we present the fabrication and characterization of isogenic scaffold-free cardiac organoids derived from human induced pluripotent stem cells (hiPSCs) formed under a supplement-deprivation regimen that allows for metabolic synchronization and maturation of hiPSC-derived cardiac cells. We propose the formation of coculture cardiac organoids that include hiPSC-derived cardiomyocytes and hiPSC-derived cardiac fibroblasts (hiPSC-CMs and hiPSC-CFs, respectively). The cardiac organoids were characterized through extensive morphological assessment, evaluation of cellular ultrastructures, and analysis of transcriptomic and electrophysiological profiles. The morphology and transcriptomic profile of the organoids were improved by coculture of hiPSC-CMs with hiPSC-CFs. Specifically, upregulation of $Ca^{2+}$ handling-related genes, such as RYR2 and SERCA, and structure-related genes, such as TNNT2 and MYH6, was observed. Additionally, the electrophysiological characterization of the organoids under supplement deprivation shows a trend for reduced conduction velocity for coculture organoids. These studies help us gain a better understanding of the role of other isogenic cells such as hiPSC-CFs in the formation of mature cardiac organoids, along with the introduction of exogenous chemical cues, such as supplement starvation.

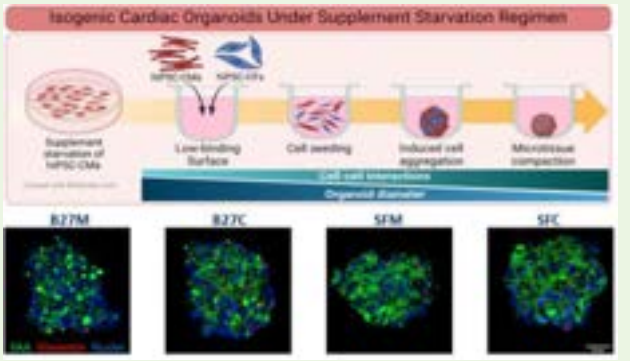


**KEYWORDS:** *cardiac organoids, isogenic engineered tissues, supplement starvation*

## 1. INTRODUCTION

Cardiovascular diseases (CVDs) have been consistently the leading cause of mortality worldwide. Additionally, the risk factors for CVDs continue to rise globally.[1] The development of novel technologies for addressing CVDs is imperative to improve the life expectancy and outcome of these diseases. Cardiac tissue engineering has emerged as a promising powerful approach to address the elevated prevalence, economic burden, and death toll caused by CVDs. However, there are remaining challenges that need to be addressed.

In the past few years, the surge and refinement of stem cell technologies have advanced the cardiac tissue engineering field. The discovery of human-induced pluripotent stem cells (hiPSCs) has allowed for the derivation of a myriad of different cell types from the same donor, namely isogenic cells. Additionally, protocols for the directed differentiation of human cardiac cells have resulted in virtually unlimited availability of cardiac cells for use in *in vitro* experimentation. However, one of the main disadvantages of using hiPSC-derived cardiac cells, and specifically hiPSC-derived cardiomyocytes (hiPSC-CMs) is their immature state and phenotype,[1−6] leading to poor representation of structural, mechanical, and electrical properties of the native heart in cellular constructs engineered from these cells.

Maturation of hiPSC-CMs is of special interest for tissue engineering due to their main role in the mechanical and electrical performance in the cardiac tissue.[7] To that end, in the past few years, numerous strategies have been proposed to improve the maturation state of hiPSC-derived cells including electrical and mechanical stimulation, prolonged culture periods and coculture with different types of cells, introduction

Received: October 30, 2022
Accepted: December 12, 2022

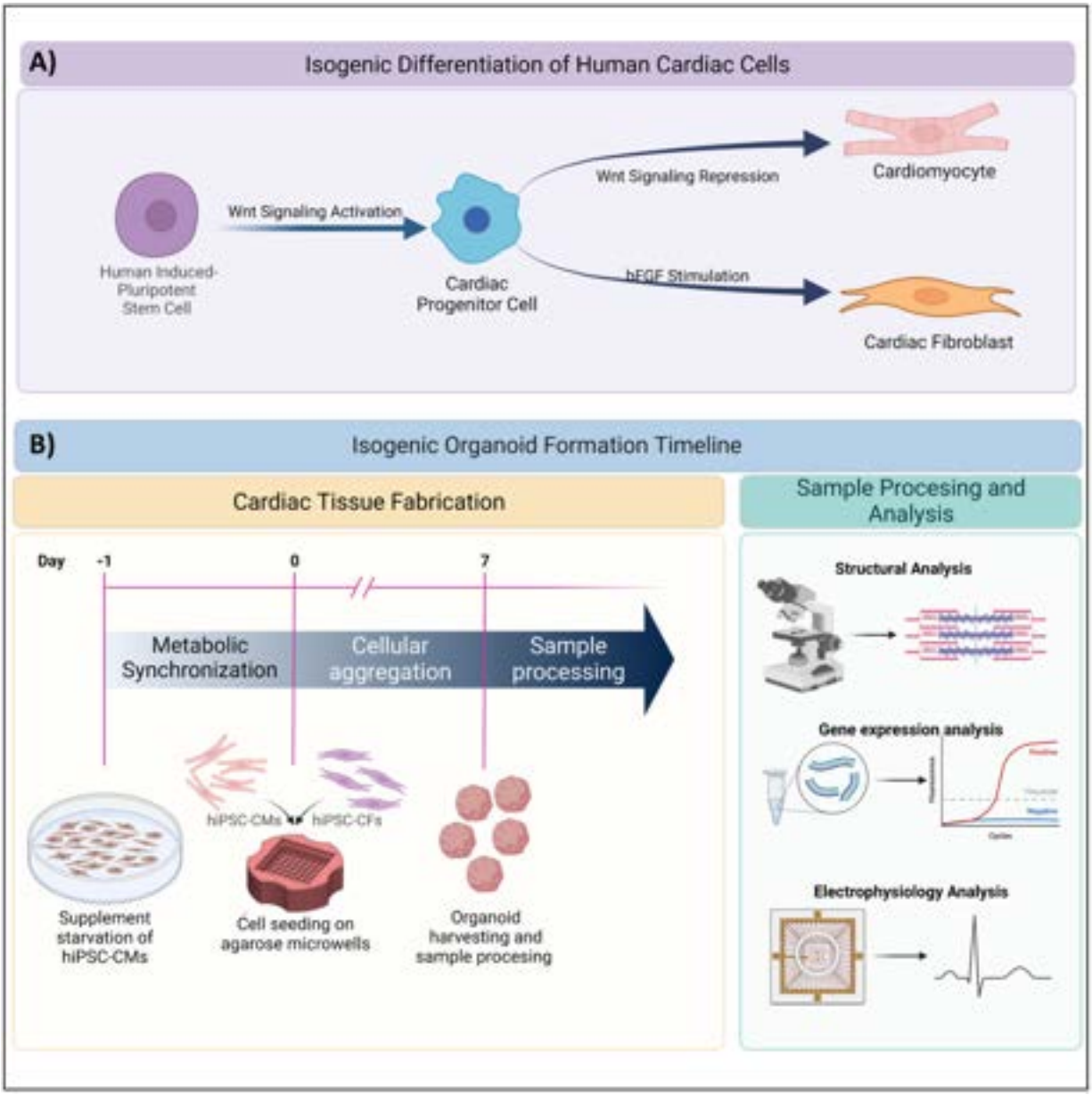


**Figure 1.** Schematic for the fabrication of scaffold-free isogenic cardiac organoids derived from human-induced pluripotent stem cells. (A) Diagram for the isogenic differentiation of cardiac cells. (B) Timeline for the fabrication of the cardiac organoids and sample processing after harvesting (created with BioRender.com).

of chemical cues such hormones and growth factors and modified topographical signaling.[8−14] Overall these findings have demonstrated that the control of the microenvironment within the engineered cardiac tissues (ECTs) is necessary for improved cell maturation and overall performance of these tissues.

The adult myocardium is formed by several types of cells. Two of the most abundant types of cells are CMs and cardiac fibroblasts (CFs). CMs generate synchronized contraction of the tissue[15] and occupy the majority of the myocardium volume.[16] While, CFs are the main producers of extracellular matrix (ECM) proteins which play an important role in the integrity of the cardiac tissue and contribute to the propagation of mechanical and electrical signaling. CFs also secrete growth factors and other signaling molecules that contribute to the cross-talk among the different cells types within the myocardium.[17] Therefore, recapitulation of cardiac tissue cellular composition is of central importance in the fabrication of physiologically relevant ECTs.[18]

The innovations in microfabrication techniques along with derivation of hiPSCs into cardiac cells have led to significant advances in the creation of cardiac organoids.[19,20] However, some characteristics of these tissues and the mechanics for their formation require further investigation. For example, the integration of isogenic cardiac cells is of very recent application and some aspects, such as cellular crosstalk and electrophysiological behavior, have not been fully evaluated yet. Additionally, there is no consensus on the optimal cellular composition of cardiac organoids.[18,21] Therefore, improving our understanding of the mechanisms for the fabrication, maturation and overall functioning of cardiac organoids requires basic investigation at the cellular and molecular level.


https://doi.org/10.1021/acsbiomaterials.2c01290
ACS Biomater. Sci. Eng. XXXX, XXX, XXX−XXX

In this study, we propose the development and characterization of scaffold-free isogenic cardiac organoids under supplement starvation regimen. There is evidence, for example, that the deprivation of serum and other supplements in the culture media can induce cellular synchronization.[22,23] Also, it has been reported that serum starvation can induce maturation of CMs derived from embryonic stem cells.[24] Conventionally, hiPSC-CMs and ECTs fabricated with these cells are maintained in a high-glucose media, and this media is enriched with a complex nutrient mixture, can support the high-metabolic need of the hiPSC-CMs.[25] Thus, it is hypothesized that replacing this nutrient-rich media with a supplement-free, low-glucose basal media can induce a latent state in the hiPSC-CMs, causing metabolic synchronization of the cell culture due to a starvation state.

We present the formation and characterization of scaffold-free isogenic cardiac organoids, fabricated with hiPSC-CMs and hiPSC-derived CFs (hiPSC-CFs). We introduce a 24 h supplement starvation regimen to hiPSC-CMs upon the formation of the cardiac organoids. The ECTs were fabricated under monoculture (only hiPSC-CMs) and coculture (hiPSC-CMs and hiPSC-CFs, 7:3 ratio respectively) conditions. We subsequently compared the phenotype and the function of cardiac organoids formed under the supplement starvation regimen to organoids formed with hiPSC-CMs that did not undergo the supplement-free period. Specifically, morphological, structural, molecular, and electrophysiological evaluation of the microtissues were performed in order to assess their maturation state, and overall performance for potential applications in cardiac repair, disease modeling, and drug screening.

## 2. EXPERIMENTAL SECTION

For the convenience of the reader, we have created a table of resources (Table S1), including all the materials used in this manuscript, along with their working concentrations and identifier numbers.

**2.1. Methods.** *2.1.1. Human Stem Cell culture.* Human-induced pluripotent stem cells (IMR90-4) were obtained from WiCell (Wisconsin, USA). The cells were cultured in mTeSR-1 media (Stem Cell Technologies) on hESC-Matrigel (Corning)-coated plates. The media was changed every day, and the cells were replated when reaching ∼80% confluency. For replating, the culture media was removed and 0.5 mM EDTA (Corning) in 1× DPBS (Dulbecco's phosphate buffered solution) was added. The cell culture was incubated with the EDTA solution for 6−7 min at room temperature. After this, the EDTA was removed, and the cells were mechanically dissociated with mTeSR-1 and replated at the desired cell density (150−250 K cells per well of a 6-well plate). Cryopreservation of the cells was performed in 90%FBS, 10%DMSO.

*2.1.2. Differentiation of hiPSC-Derived Cardiomyocytes.* The differentiation of the hiPSC-CMs was performed under the GiWi protocol.[25] This protocol is specific for ventricular CMs and is based in the introduction of small molecules for the regulation of the canonical Wnt signaling. The differentiation process was started when the hiPSCs reached at least 80% confluency. On day 0 (D0) the culture media was changed to RPMI+B27 minus insulin (RPMI 1640, 2%B27 minus insulin (Gibco), 1%Pen/Strep (Gibco)). Additionally, 7−9 $\mu$M CHIR99021 (BioVision) was integrated to the media in order to inhibit the Glycogen Synthase Kinase-3 (GSK) pathway and activate the canonical Wnt pathway. Exactly 24 h later (day 1), the media was changed to RPMI+B27 minus insulin. Seventy-two hours postinitiation of the differentiation (day 3), a 1:1 mixture of conditioned media from the cell culture and fresh RPMI+B27 minus insulin was supplemented with 5 $\mu$M IWP-2 (Sigma) for inducing the inhibition of the Wnt pathway in the cells. On day 5, the media was changed to RPMI+B27 minus insulin to allow for cell recovery. After this, the media was changed every 48 h with RPMI +B27 to promote cell maturation (Figure 1A). The hiPSC-CMs presented spontaneous beating typically around day 9 (Video S1)

In order to increase the yield of the differentiation of the hiPSC-CMs, on day 13, glucose-free media (RPMI 1640 minus glucose, B27, 4 mM sodium lactate, 1%Pen/Strep) was used to allow for hiPSC-CM enrichment through glucose starvation.[4] The media was changed every 72 h. On day 19, the media was switched to RPMI+B27 to allow for cell recovery. After this, the obtained hiPSC-CMs were dissociated using TrypLE Express (LifeTech) and replated in Matrigel-coated plates. Following this, the media was changed every 48 h upon starting all the experiments.

*2.1.3. Differentiation of hiPSC-Derived Cardiac Fibroblasts.* The differentiation of hiPSC-CF was based in the consecutive modulation of the canonical Wnt and fibroblast growth factor (FGF) signaling through the introduction of small molecules and growth factors to the culture medium.[26] The hiPSCs were allowed to reach at least 80% confluency before starting the differentiation process. The hiPSC-CFs differentiation protocol was started by changing cell culture medium for RPMI+B27 minus insulin, conditioned with 7 $\mu$M CHIR99021 (BioVision). On day 1, culture media was changed to RPMI+B27 minus insulin simple to allow for cell to recovery.

On day 2 of the differentiation the medium was changed to the basal CF differentiation medium, consisting of high glucose (4.5 g/L) DMEM with L-glutamine (4 mM) (Gibco), and complemented with HLL supplement (human serum albumin (500 $\mu$g/mL), linoleic acid (0.6 $\mu$M), and lecithin (0.6 $\mu$g/mL). This medium was supplemented with 70 ng/$\mu$L $\beta$-fibroblast growth factor ($\beta$-FGF). Next, the culture media was changed every 48 h with basal CF differentiation medium supplemented with $\beta$-FGF (70 ng/$\mu$L). The hiPSC-CFs were dissociated with 1× Trypsin and replated on uncoated plates on day 20. From this point the cells were maintained with fibroblast growth media-3 (FGM-3) (Fisher Scientific), changing the medium every 48 h. The fibroblasts were passaged when they reached ∼85% confluency. Freezing media was composed by 80%FGM3, 10%FBS, and 10%DMSO. For all of our experiments, hiPSC-CFs were used between passage numbers P8 and P12 to avoid the differentiation of the CFs into myofibroblasts.

*2.1.4. Supplement Starvation Regimen for hiPSC-CMs.* Prior to the formation of the cardiac organoids, the hiPSC-CM were introduced to a 24-h supplement-free period to induce the metabolic synchronization of the cellular population due to low availability of nutrients.[22,23] On day 25 after initiated the hiPSC-CM differentiation, the cells were washed with 1× DPBS twice. Then, the basal culture media was substituted by serum free medium (serum-free Dulbecco's modified Eagle's medium (DMEM) supplemented with glucose (4.5 g/L), L-glutamine (584 mg/L), and sodium pyruvate (110 mg/L)). After exactly 24 h, these cells were used for the formation of the cardiac organoids (Videos S2 and S3).

*2.1.5. Casting of Agarose Microwells.* The cardiac organoids were fabricated using agarose microwells (800 $\mu$m diameter, 800 $\mu$m depth). The microwells were casted using commercially available silicon molds (Microtissues), yielding to 35-microwell devices. For this, a solution of 2% agarose in sterile saline (0.9% (w/v) NaCl) was prepared. Then, 330 $\mu$L of the agarose solution were deposited in the silicon molds and allowed to solidify at room temperature. The agarose microwells were demolded carefully, placed in 24-well culture plates, and 1 mL of RPMI+B27 plus insulin was deposited in each well. The microwells were incubated for at least 1 h at 37 °C to allow the conditioning of the microwells, this step was repeated one more time before using the microwells for cardiac tissue formation.

*2.1.6. Fabrication of Scaffold-Free Cardiac Organoids.* The hiPSC-CMs were dissociated using TrypLE Express for 12 min at 37 °C followed by mechanical dissociation with a micropipette. After this, the TrypLE Express was neutralized with basal culture medium and the cells were centrifuged at 300g for 3 min. The supernatant was replaced by basal RPMI 1640 medium. Likewise, the hiPSC-CFs were dissociated from the culture plates by using 0.05% Trypsin-EDTA (Thermo) and incubated for 3−4 min at 37 °C. After mechanical


https://doi.org/10.1021/acsbiomaterials.2c01290
ACS Biomater. Sci. Eng. XXXX, XXX, XXX−XXX

dissociation, the trypsin was neutralized with FGM3 and the cells were centrifuged at 250g for 4 min. For monoculture organoids, hiPSC-CM were resuspended at a concentration of 175 × $10^3$ cells per 75 μL of basal RPMI 1640 medium. For coculture organoids, the cells were mixed at a ratio of 70%:30% hiPSC-CM and hiPSC-CFs, respectively, to an equal concentration of 175 × $10^3$ cells per 75 μL, with the aim of creating cardiac organoids of 5 × $10^3$ cardiac cells each. The cellular ratio for the coculture organoids was carefully selected after the extensive optimization experiments of the proportion of the cellular population (data not shown).

The cells were allowed to sit undisturbed in the agarose microwells for 1 h at 37 °C before adding 1 mL of basal RPMI medium to each well. After this, the culture media was changed every 48 h. The cardiac organoids were allowed to aggregate in the agarose microwells for 7 days before harvesting (Figure 1B, Videos S4−S7). Four different experimental conditions were produced as follows:

- B27M: Monoculture organoids formed with supplemented hiPSC-CMs.
- B27C: Coculture organoids formed with supplemented hiPSC-CMs and hiPSC-CFs.
- SFM: Monoculture organoids, formed with supplement-free hiPSC-CMs.
- SFC: Coculture organoids, formed with supplement-free hiPSC-CMs and hiPSC-CFs.

*2.1.7. Microscopy Imaging and Morphological Characterization.* Phase-contrast and fluorescence images were acquired by Zeiss Axio Observer Z1 equipped with Apotome2 (Zeiss) and ZenPro software. The samples were imaged at 2.5× in the agarose microwells on day 1 and day 7 after seeding the cells in order to track the size change. Additionally, on day 7, time-lapse imaging of individual organoids was recorded at 10× for 20 s at 34 °C for spontaneous beating behavior characterization. Time-lapse images were analyzed with a custom MATLAB code in order to extract the spontaneous beating rate. Also, the interbeat intervals were measured from the extracted signals; then interbeat interval variability (IIV) parameter was calculated as the standard deviation of this measure. We performed one-way ANOVA analysis to the extracted beating rate and IIV signals in order to evaluate the statistical differences between groups.

Morphological characterization of the cardiac organoids was performed by analyzing and processing the phase-contrast images with the "Measure" and "Shape descriptors" tools of FIJI software.[27−29] Specifically, tracing straight lines for measuring the diameter and using the "freehand selection" tool to trace the edges of individual organoids.[30] A total of 15−20 cardiac organoids were evaluated per experimental group. A total of three biological replicates ($N$ = 3) were evaluated in order to perform statistical analysis.

*2.1.8. Cardiac Organoid Cryosectioning.* In order to perform the immunohistochemistry (IHC), the formed tissues were cryosectioned. First, the cardiac organoids were harvested on day 7 after seeding in the agarose microwells. The samples were washed with 1× DPBS to remove cellular debris accumulated in the agarose microwells. Then, the tissues were fixed with 4% paraformaldehyde (4% PFA) (ThermoScientific) for 45 min at 37 °C. Next, the samples were rinsed twice with PBS-glycine (100 mM), followed by one rinse with PBS-Tween20 (0.05% (v/v)).

To prevent ice crystal formation when freezing the cardiac organoids, sucrose cryoprotection was performed. Briefly, after the PBS-Tween 20 wash, the tissues were submerged in a solution of 15%(w/v) sucrose in DI water for 1 h at room temperature. Then, the sucrose solution was replaced by a 30%(w/v) sucrose solution overnight at 4 °C. The next day, the sucrose solution was removed, and the tissues were fast-frozen by embedding in Tissue-Tek OCT compound (Tissue-Tek). The OCT-embedded tissues were deposited in specimen holders and then placed in a freezing bath formed with 95% ethanol and dry ice nuggets. The OCT was allowed to completely solidify before removing from the ethanol bath. The samples were preserved at −80 °C until ready for cryosectioning.

The cryosectioning was performed with the CryoStar NX70 cryostat (ThermoScientific). It was setup to make tissue slices of a thickness of 10 μm. With the holder at a temperature of −10 °C and the blade at −14 °C. The tissue slices were collected in positively charged glass slides and were preserved at −20 °C until further processing.

*2.1.9. Immunohistochemistry.* After cryosectioning, the tissue slices were rinse once with PBS-Tween 20 to eliminate remaining OCT from the glass slides. The tissues were permeabilized using an IF buffer (0.2% Triton X-100, 0.1% BSA (radioimmunoassay grade), 0.05% Tween 20, 0.02% NaN3 in 1× DPBS) for 30 min at room temperature. In order to prevent unspecific antibody binding, sample blocking was performed with 10% goat serum (ImmunoReagents) for 1 h at room temperature. Primary antibodies were diluted in 10% goat serum as follow: sarcomeric alpha actinin (SAA) (Thermo Fisher, Cat#: MA1-22863) 1:100; Connexin 43 (Abcam, Cat#: ab11370) 1:125; Vimentin (Cell Signaling, Cat#: D24H3) 1:100. The samples were incubated at 4 °C overnight with the primary antibody solution; a sample incubated with only 10% goat serum was used as secondary antibody control.

The next day, the samples were washed with DPBS-Tween20 for 15 min four times at room temperature. The secondary antibodies and 4′,6-diamidino-1-phenylindole (DAPI) were diluted in 1x DPBS (1:500 and 1:1000, respectively) and the solution was centrifuged at 14,000 rpm for 10 min in order to eliminate antibody aggregates. The secondary antibodies plus DAPI were added to the samples and incubated for 1 h at 37 °C. Finally, the samples were washed three times with 1× DPBS-Tween20 for 15 min protected from light. The samples were mounted using VectaShield (Vector) to prevent fading and bleaching of the fluorophores. Imaging was performed with the Leica SP8 Confocal Microscope at 63× and 100×. The z-stack projection was then reconstructed using FIJI software. The assay was repeated for $N$ = 3 biological replicates.

In order to evaluate the sarcomere length of the hiPSC-CMs within the cardiac organoids the "Measure" tool of the FIJI software was used. Individual sarcomere lengths were measured by tracing a straight line from consecutive Z-discs, stained with the anti-SAA antibody as shown in Figure S4. A total of 35−50 measurements per experimental group, per biological replicate were calculated in order to performed the statistical analysis.

*2.1.10. TUNEL Assay.* The samples for TUNEL assay were harvested from the agarose microwells on day 7 after seeding. Then, the samples were fixed and cryosectioned, and stained using the commercially available Click-iT Plus TUNEL assay (Invitrogen), following the instructions indicated by the kit. Briefly, the samples were permeabilized with a proteinase-K solution. Followed by a DI water rinse and incubation with the TdT buffer for 10 min. Then, the TdT solution was added to the samples and incubated for 60 min. Next, the samples were rinsed with DI water and 3% BSA, 0.1% TritonX-100 in PBS. The Click-iT Plus TUNEL reaction cocktail was added to the samples and incubated for 30 min. After rinsing, a DAPI staining was performed for 15 min. All the incubations were completed at 37 °C. A sample treated with DNase-1 for 30 min was used as positive control. The samples were imaged with the Zeiss Axio Observer Z1 microscope equipped with Apotome2 (Zeiss) and ZenPro software at 20×. The $z$-stack projections were reconstructed with FIJI software. The assay was repeated for $N$ = 3 biological replicates.

*2.1.11. Quantitative Real-Time Reverse Transcription-PCR (qRT-PCR).* After 7 days in the agarose microwells the cardiac organoids were harvested and rinsed twice with 1x DPBS to eliminate cellular debris accumulated in the microwells. After this, the RNA from the samples was extracted using the RNA MicroPrep kit (Zymo). The RNA quality and concentrations were evaluated using the NanoDrop UV−vis Spectrophotometer. Nuclease-free (NF) water was used as a blank, then 2 μL of the sample was used for the measurement. Total RNA was used for the cDNA synthesis along with iScript Reverse Transcription Supermix (BioRad).

For qRT-PCR, melting curve analysis and PCR product size quantification were used for primer validation (Table S2). 18S was used as the housekeeping gene for dCt normalization as previously optimized by our group.[8] A qPCR master mix reaction was created by


https://doi.org/10.1021/acsbiomaterials.2c01290
ACS Biomater. Sci. Eng. XXXX, XXX, XXX−XXX

combining the 5 $\mu$L of iTaq Universal SYBR Green Supermix (BioRad), 3.9 $\mu$L of NF water, 0.1 $\mu$L of the cDNA sample, and 1 $\mu$L of the primer working solution (8 $\mu$M of forward and reverse primers in NF water). The qRT-PCR reactions were performed in 96-wells plates using the q-Tower real time thermocycler (Analitik Jena). All dCt values were normalized to the respective sample collected on D-1 (before starting supplement starvation). The assay was repeated for $N$ = 3 biological replicates.

*2.1.12. Microelectrode Array (MEA) Electrophysiological Analysis.* Glass microelectrode arrays (MEAs) with 59 electrodes plus one reference electrode were used for the MEA electrophysiological analysis (Naturmedizinisches Institute (NMI) of the University of Tubingen). The array consists of an 8 × 8 grid of electrodes, spaced by 200 $\mu$m (center-to-center), with a recording diameter of 30 $\mu$m. The MEAs were prepared prior the electrophysiology analysis to allow for adhesion of the cardiac organoids to the surface and induce the contact of the cardiac cells with the microelectrodes. First the devices were sterilized with UV-radiation for at least 1 h. Then, the MEAs were rinsed twice with DI water. The MEAs were coated with Matrigel (Corning) overnight at 37 °C to provide anchorage sites to the cells. After harvesting, the tissues were rinsed twice with 1× DPBS. Then, the cardiac organoids were deposited on the MEA devices with RPMI basal media. The devices were swirled gently to promote the localization of the cardiac tissues on top the electrodes and ensure the acquisition of the electrophysiological signals. The organoids were allowed to sit undisturbed for at least 24 h before the electrophysiological signal acquisition.

The electrophysiology module from LLC with a interface board (PLEXON) and temperature control (BMSEED LLC.) was used for obtaining the signals from the MEAs. The INTAN Stimulation/Recording controller was used in combination with the RHX software as the user interface. The field potentials (FPs) of spontaneous beating signals were recorded for 30 s for each sample. The signals were mapped by correlation with phase contrast images at 2.5× (Zeiss Axio Observer Z1 microscope and ZenPro software) and analyzed using a custom MATLAB code.

Regions of interest (ROIs) for the evaluation of electrophysiological signals were determined through the creation of FPs heatmaps. ROIs were selected as the more active areas according to the FPs heatmaps and corroborated with phase-contrast imaging as the electrodes that were in contact with localized organoids. The conduction velocity (CV) was calculated by first measuring the signal propagation time ($\Delta t_{\text{average}}$) between channels within the ROIs. For this, the time of occurrence for beating peaks was detected for all ROIs, then $\Delta t$ was calculated by

$$\Delta t = |t_{\text{ocurrence of Channel A}} - t_{\text{ocurrence of Channel B}}| \quad (1)$$

Then

$$\Delta t_{\text{average}} = \frac{1}{n}\sum_{i=1}^{n} \Delta t \quad (2)$$

where $n$ is the number of peaks detected per channel. The CV for a pair of channels was calculated by

$$\text{CV}_{\text{AB}} = \frac{\text{distance between channels}}{\Delta t_{\text{average}}} \quad (3)$$

Finally, the average CV per ROI was calculated as the average of all the $\text{CV}_{\text{AB}}$ values found within the ROI. The CV of 2 to 3 ROIs was averaged per sample, and this was taken as the CV of the sample. $\text{CV}_{\text{AB}}$ value outliers were identified through Grubb's test (GraphPad Prism) and were not used for the calculation of the final CV.

*2.1.13. Statistical Analysis.* All the statistical analyses were carried using GraphPad Prism. Two-way ANOVA was used for analyzing the diameter changed of the cardiac organoids. One-way ANOVA was performed in circularity and roundness analysis, as well as for qRT-PCR. A two-tailed $t$ test was used for analysis of the CV. Significance level was of $\alpha$ = 0.05 for all cases. All results are presented in the form of mean ± SEM. A minimum of three biological replicates ($N$ = 3) were analyzed for all the experimental assays, except for MEA analysis, for which two biological replicates ($N$ = 2) were utilized for the experiments.

**2.2. Results and Discussion.** *2.2.1. Isogenic Differentiation of hiPSC-Derived Cardiomyocytes and Cardiac Fibroblasts.* Derivation of cardiac cells from one hiPSC source, namely, isogenic cardiac cells, is of relevance for several applications within the cardiac engineering field.[31] On the one hand, it allows for the creation of ECTs fabricated with different types of cells, contributing to a closer resemblance of the native myocardium composition. Additionally, the inclusion of different types of cardiac cells allows for cell-to-cell communication through growth factors, cytokines, and other chemical cues that promote maturation of the ECTs.[32]

Moreover, multicellular ECTs are of physiological relevance for numerous *in vitro* applications. For instance, while CMs are responsible of the contraction and main mechanical function of the heart, a number of cardiac diseases are mediated by the activation of CFs and their deposition of ECM proteins.[33] Therefore, *in vitro* models that accurately recapitulate myocardium cellular composition are necessary for disease modeling and drug screening applications. Moreover, the potential for using patient-derived cells in the ECTs can help to overcome challenges such as engraftment to the host myocardium and biocompatibility and rejection issues.

The cardiac cells utilized herein for the formation of the cardiac organoids were obtained from the differentiation of hiPSC monolayers (Figure 1A). The selected cell line presented a pluripotency state (Figure S1A) that allowed for the induction of the hiPSCs into cardiogenic mesodermal progenitor cells through the activation of the canonical Wnt signaling. This activation was mediated by the introduction of the CHIR99021 small molecule. Further chemical cues allowed for the successful derivation of CMs and CFs. For example, the introduction of the IWP-2 small molecule on D3 after initiated the differentiation acts repressing the Wnt signaling, which leads to the commitment of the cells toward a cardiac progenitor cell fate, and finally CMs with immature state.[34] On the other side, the presence of FGF in the environment of cardiac mesodermal progenitor cells interacts with the BMP signaling, directing the cells to a nonmyocyte fate, thus leading to the commitment toward CFs.[26]

Based on our utilized protocol, typically the hiPSC-CMs presented spontaneous beating around day 10 after the initiation of differentiation. After metabolic selection through glucose starvation and replating of the cells, we obtained uniform monolayers of beating cells (Video S1). Besides the spontaneous beating, the successful differentiation of hiPSC-CMs was confirmed through immunostaining for cardiac relevant markers, such as SAA. Additionally, the yield of our differentiation protocol (>90% hiPSC-CMs) has been analyzed by flow cytometry previously.[8] The differentiation of the hiPSC-CFs was validated by cell morphology evaluation and immunostaining for TE7 and vimentin (Figure S1B).

It has been reported that supplement starvation can help with hiPSC-CM maturation by inducing structural and metabolic changes, and overall improved performance of ECTs.[22−24] Traditional protocols for differentiation of hiPSC-CMs require RPMI 1640 with B27 supplement as basal cell culture media for cell maintenance after day seven of differentiation. B27 is a serum-free supplement that was originally formulated and optimized by Brewer et al. for the survival of hippocampal neurons.[35,36] It contains antioxidants, proteins, fatty acids, and vitamins that help support cells in a neonatal state. The metabolism of hiPSC-CMs is dependent on the presence of fatty acids, among other nutrients, and it has been reported that the change in the culture media composition can lead to changes in the metabolism of neonatal CMs.[37] Thus, it was shown that nutrient deprivation can lead to a homogeneous cell culture composition, via metabolic cell synchronization.[23] By substituting the basal culture media with a supplement-free media we aimed to induce a metabolic shift in the hiPSC-CMs, as it has been previously demonstrated that nutrient deprivation leads to cellular maturation.[24]

*2.2.2. Formation of Isogenic Cardiac Organoids.* When forming scaffold-free ECTs, cellular aggregation is an important consideration. The lack of a matrix that provides mechanical support to the cells can


https://doi.org/10.1021/acsbiomaterials.2c01290
ACS Biomater. Sci. Eng. XXXX, XXX, XXX−XXX

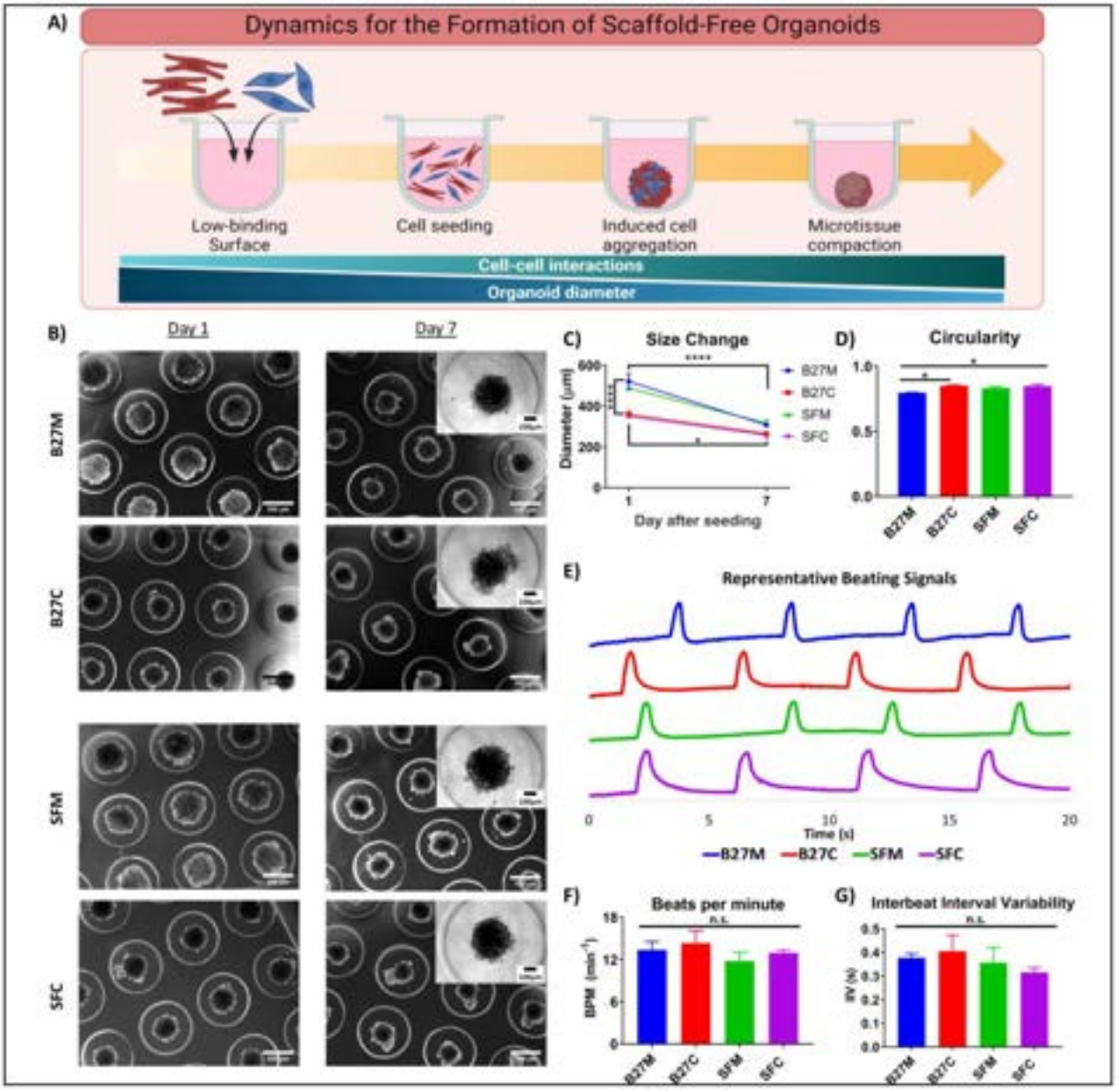


**Figure 2.** Morphological characterization of the isogenic cardiac organoids from phase-contrast imaging. (A) Schematic representation of induced cell aggregation and compaction of isogenic cardiac organoids, showing increased intercellular interactions and decreased diameter with time progression (created with Biorender.com). (B) Representative phase-contrast images of the formed organoids (day 1 vs day 7 after seeding) (scale bars: 500 $\mu$m). Insets: 10× phase-contrast images of single cardiac organoids on day 7 (Inset scale bar: 100 $\mu$m). (C) Size change of the cardiac organoids (day 1 vs day 7 after seeding). (D) Circularity evaluation of the cardiac organoids, measured on day 7 after seeding. (E) Normalized representative spontaneous beating signals extracted from phase-contrast videos (*Y*-axis represents arbitrary units). (F) Spontaneous beating rate of the cardiac organoids. (G) Interbeat interval variability calculated from the spontaneous beating signals obtained from the cardiac organoids. One-way ANOVA was performed for all the evaluations (n.s. = *P*-value > 0.05, * = *P*-value ≤ 0.05, **** = *P*-value ≤ 0.0001). Abbreviations: B27M, monoculture supplemented organoids; B27C, coculture supplemented organoids; SFM, supplement starved monoculture organoids; SFC, supplement starved coculture organoids.

ultimately lead to induction of apoptosis through anoikis,[38,39] causing the failure of the ECTs. Additionally, cell coupling within the ECTs allows for the propagation of chemical, electrical, and mechanical cues that are necessary for their proper function.[19] Therefore, it is necessary to evaluate the cellular aggregation of the cardiac organoids in order to elucidate the effects of the coculture and supplement-free regimen. Despite the importance of cellular aggregation in scaffold-free cardiac tissues, the progressive change in size of cardiac organoids has not been thoroughly described previously and it is often overlooked, focusing only on the final size of cardiac organoids. However, the progressive size change can be helpful to characterize the dynamics of cellular adhesions and aggregation, contingent upon the different cellular compositions in ECTs. In this study, we performed a 24 h supplement starvation regimen for the hiPSC-CMs prior to the formation of the scaffold-free cardiac organoids (Figure 1B, Figure S2A). Additionally, we fabricated coculture cardiac organoids, formed with 70% hiPSC-CMs and 30% hiPSC-CFs. We hypothesized that the supplement starvation regimen in conjugation with coculture with hiPSC-CFs will lead to an improved formation and functionality of the cardiac organoids.

Phase-contrast imaging and video recordings were used to evaluate the morphology of the cardiac organoids (Figure S2B). The diameter


https://doi.org/10.1021/acsbiomaterials.2c01290
ACS Biomater. Sci. Eng. XXXX, XXX, XXX−XXX

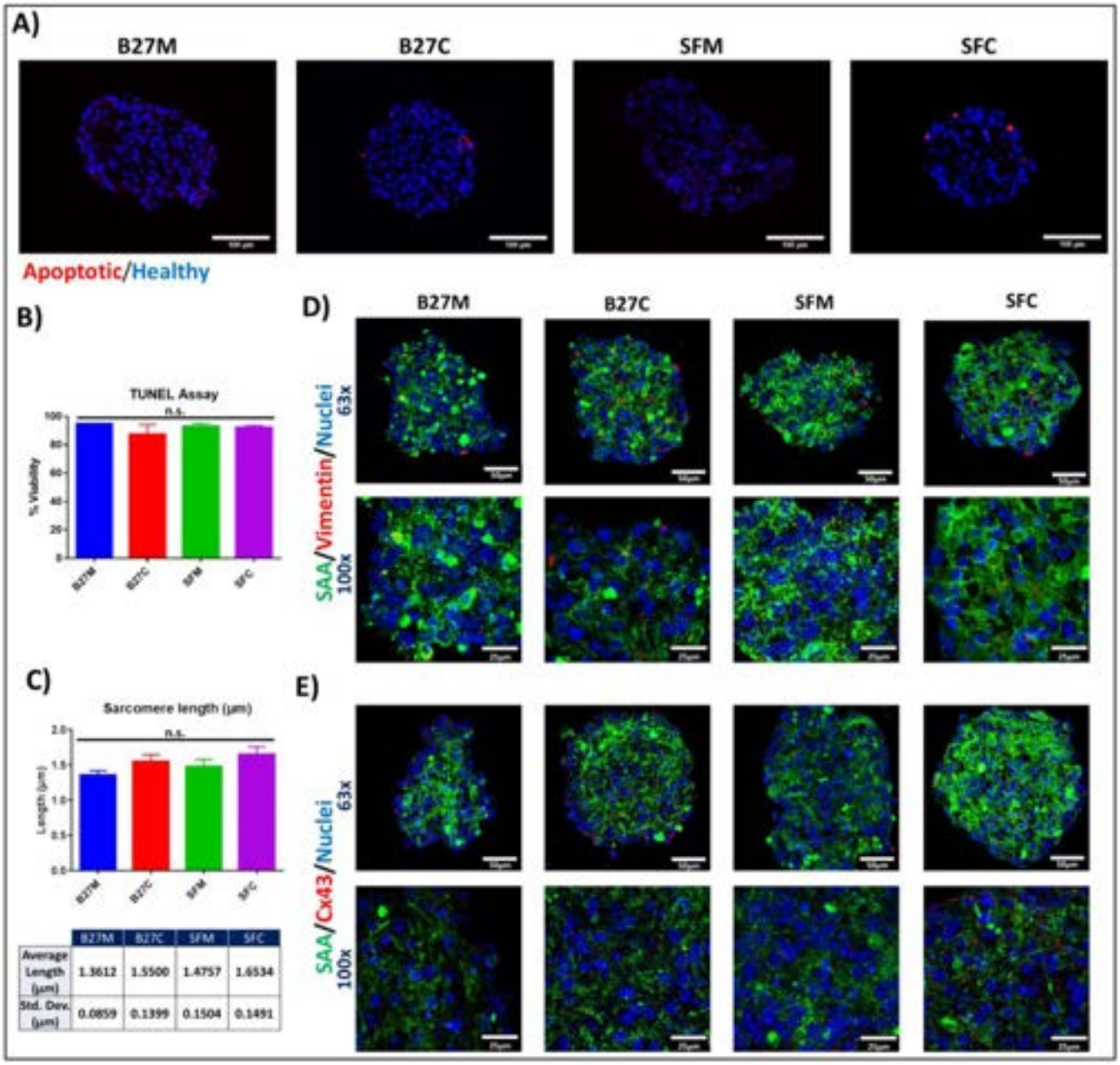


**Figure 3.** Structural characterization of the isogenic cardiac organoids from confocal imaging. (A) Representative images for TUNEL assay performed over cryosectioned slices of the cardiac organoids on day 7 after seeding (red, apoptotic cells; blue, healthy cells) (Scale bars: 100 $\mu$m). (B) Viability evaluation based on TUNEL assay. No significant cell death was found on any of the experimental conditions. One-way ANOVA was performed for all the evaluations (n.s. = $P$-value > 0.05). (C) Quantification of sarcomere length based on IHC images of cardiac organoids (n.s. = $P$-value > 0.05). (D) Confocal imaging of 10 $\mu$m cryosectioned slices of the cardiac organoids on day 7 after seeding. Top row: 63× magnification (scale bar: 50 $\mu$m). Bottom row: 100× magnification (scale bar: 25 $\mu$m) (green, sarcomeric alpha actinin; red, vimentin; blue, nuclei). (E) Confocal imaging of IHC stained cryosectioned cardiac organoids for the visualization of the sarcomeric structures and Cx43 expression (green, SAA; red, Cx43; blue, nuclei) (top row scale bars, 50 $\mu$m; bottom row scale bars, 25 $\mu$m).

change of the microtissues was monitored within the agarose microwells from day 1 to day 7 after cell seeding. Briefly, the interfacial tensions between the agarose microwells surface and the culture media along with a relatively high availability of adhesion proteins (connexins and cadherins) promote the adhesion between the cells, leading to the formation of self-arranged ECTs (Figure 2A, Videos S4−S7). The cardiac organoids retained their morphology and size after harvesting from the agarose microwells, confirming the formation of cell−cell adhesions.

We observed an important change in the overall shape and size of the organoids from day one to day seven (Figure 2B, C). First, we found that the final organoid diameter at day seven was similar for all the experimental conditions. However, diameter evaluation at day 1 after seeding in the agarose microwells, showed a significantly reduced size for the coculture groups B27C and SFC (Figure 2C). This suggests that the presence of hiPSC-CFs in the ECTs promotes an accelerated cellular aggregation and microtissue compaction. Earlier cellular aggregation can be beneficial in the formation of cardiac organoids. First, the physical cell-to-cell adhesions and communication can help with cell survival by preventing anoikis.[39] Second, it has been previously demonstrated that CFs can deposit ECM proteins[17] that can also help with cell support and mechanical signal


https://doi.org/10.1021/acsbiomaterials.2c01290
ACS Biomater. Sci. Eng. XXXX, XXX, XXX−XXX

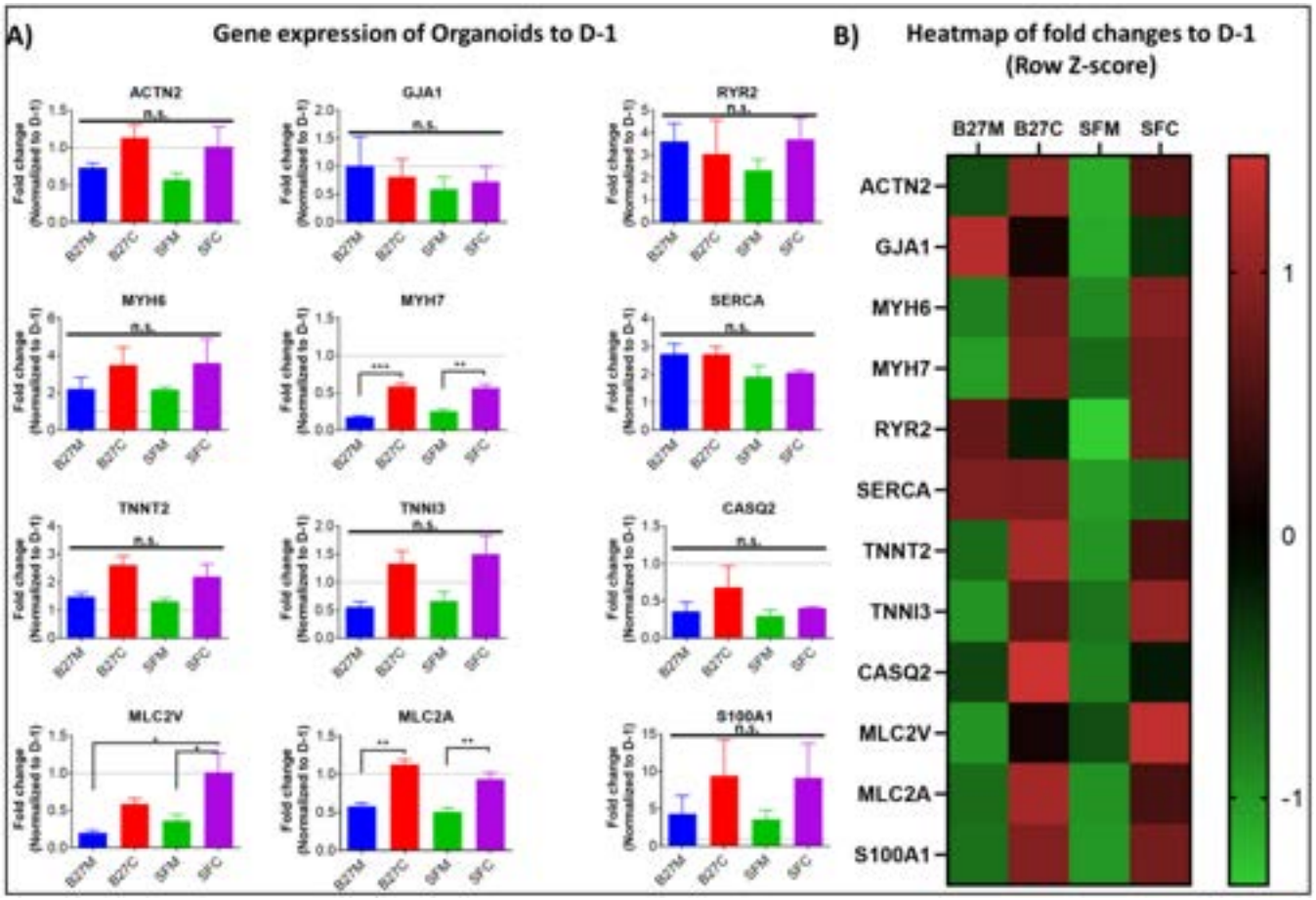


**Figure 4.** Gene expression profile of the isogenic cardiac organoids on day 7 after seeding. (A) Fold-change values of a panel of 12 cardiac-relevant genes, evaluated through qRT-PCR. All the results from the experimental conditions were compared to the day before starting the supplement starvation (namely, D-1). One-way ANOVA was performed for finding statistical differences (n.s. = *P*-value > 0.05, * = *P*-value .05, ** = *P*-value ≤ 0.01, *** = *P*-value ≤ 0.001). (B) Heatmap for Z-score of gene expression of cardiac-relevant genes. A trend for higher expression on the coculture conditions is shown.

propagation. Thus, the presence of hiPSC-CFs in the formation of the cardiac organoids was seen to be beneficial for a rapid induced cellular aggregation, leading to the microtissue compaction and resulting in a decrease in the size of the ECTs with time progression.

Circularity evaluation of the organoids on day seven revealed that B27C and SFC groups present a significantly more circular shape and smoother edges (Figure 2D). Smoother organoid edges could be indicative of improved cellular compaction, which leads to a higher cell density within the ECTs, resulting in organoids of physiological-relevant cellular density. Additionally, the coculture groups showed a more circular morphology when compared to their monoculture counterparts.

A more rounded morphology and overall higher shape homogeneity across cardiac organoids could be beneficial for several applications.[40−42] For example, the use of cardiac organoids has been proposed as the building blocks for bioprinting of large-scale cardiac tissues.[43] Thus, derivation of compact organoids with low diameter variability and reproducible size will be optimal for 3D bioprinting processes. Additionally, rounder morphology, greater compaction, and increased cellular density could facilitate the injection, survival, and engraftment of cardiac organoids within the diseased myocardium when used for cardiac repair and replacement.

After analyzing the spontaneous beating signals extracted from the phase-contrast videos, we found a similar beating pattern for all the experimental conditions (Figure 2E). The calculated spontaneous beating rates (BPM) did not show significant differences between any of the groups (B27M, 13.4 ± 1.7; B27C, 14.3 ± 2.5; SFM, 11.8 ± 1.8; SFC, 12.9 ± 0.6) (Figure 2F). Interbeat interval variability (IIV) was calculated as the variation in the duration of the beat-to-beat intervals in the extracted signals (Figure 2G). IIV is a measure of the periodic contractions of the cardiac tissue and has been used as a parameter to evaluate the synchronicity of the tissues, and as indirect measurement of mechanical and electrical coupling of the cardiac cells. Our evaluation did not show any significant difference between experimental groups, suggesting a similar degree of cell-to-cell coupling, regardless of the cellular composition of the cardiac organoids.

*2.2.3. Evaluation of the Cellular Ultrastructure of Cardiac Organoids.* Some of the main challenges for engineering scaffold-free cardiac tissues is the limitation in size due to the lack of vascularization, the oxygen diffusion limit, and meeting the metabolic requirements of the hiPSC-CMs.[44−46] To evaluate cell survival within the cardiac organoids, we performed a TUNEL assay on cryosectioned slices of tissues harvested on day seven after seeding to evaluate early apoptotic cells (Figure 3A). We did not find significant cell death for any of the conditions (Figure 3B), suggesting that the size of the organoids allowed for the adequate oxygen and nutrient diffusion and that the cells remained viable after the collection of the microtissues.

Through confocal imaging, we observed the cellular ultrastructures of the cardiac organoids. Specifically, when costaining the ECTs for cardiac biomarkers we were able to simultaneously visualize distinct cellular components that allowed for the structural characterization of the organoids. First, we performed immunohistochemistry (IHC) costaining for sarcomeric alpha actinin (SAA) and vimentin in order to evaluate the cellular composition and distribution within the ECTs.


https://doi.org/10.1021/acsbiomaterials.2c01290
ACS Biomater. Sci. Eng. XXXX, XXX, XXX−XXX

SAA is one of the vital protein components of the sarcomeric unit for mechanotransduction and is used as a gold standard biomarker for hiPSC-CMs. Additionally, vimentin is a structural protein that can be found within cardiac fibroblasts and is responsible for cell shape stabilization and cytoplasm integrity. Consequently, vimentin has been widely used as a biomarker for CFs.[17]

One of the main attributes of the immature phenotype of hiPSC-CMs is poor sarcomeric structure development. Sarcomeres are the leading structures in the mechanical functioning of the myocardium, critical in the synchronized contraction and relaxation of the cardiac muscle.[47,48] Mature contractile machinery in CMs is characterized by the presence of elongated and robust sarcomeric units. SAA is found intertwined with myosin and actin within the sarcomeric unit and is localized in the so-called Z-discs.[49]

Thus, when CMs are stained against SAA, the cells present striation bands that are perpendicular to the main axis of the body of the cells. All our experimental groups showed these characteristic structures, with regions across all of the body of the organoids where SAA bands are present. These SAA bands correspond to the Z-discs of the sarcomeric structures and serve as a biomarker to detect the distribution of the hiPSC-CMs. Quantification of the sarcomere length, which is the average distance from band to band, showed an average length ranging from 1.36 to 1.65 $\mu$m for all the groups. Although the statistical analysis did not show significant differences, there is an apparent trend for an increase sarcomere length in the coculture groups (Figure 3C). The stained hiPSC-CMs can be observed oriented in arbitrary positions within the organoids. Since the cellular aggregation of the ECTs was not directed by any external physical or chemical cue, cellular alignment was not anticipated. Moreover, SAA distribution is similar for all the experimental conditions (Figure 3D).

As expected, higher expression of vimentin was found in the coculture organoids (B27C and SFC) by the enrichment of hiPSC-CFs in the formation of these. Similar to the distribution of the hiPSC-CMs, the presence of vimentin in the ECTs does not follow a specific alignment or localization, and it was observed throughout the entire cross-section of the organoids (Figure 3D). A modest expression of vimentin in the monoculture cardiac organoids (B27M and SFM) was observed. While our directed differentiation protocol and further metabolic selection of hiPSC-CMs has a high production yield (>90% hiPSC-CMS),[8] it is possible that hiPSC-CFs and other cell types that are not specified were generated as a byproduct of the CMs differentiation and that these cells survived the glucose starvation; thus, remaining present in the final form of the organoids.

The formation of cell-to-cell adhesions is vital for the fabrication of scaffold-free ECTs. In the native cardiac tissue, cells can be found forming a single syncytium that can conduct mechanical and electrical cues.[50−52] The propagation of electrical signals is mainly due to the depolarization and repolarization of the cell membrane.[52] Thus, the formation of gap junctions is a main focus for the characterization of cardiac organoids since they are the main mechanism for electrical conduction in the cardiac tissue. One of the main gap junction proteins, expressed both by CMs and CFs, is connexin 43 (Cx43). Therefore, IHC costaining of SAA and Cx43 was used to visualize the expression and localization of gap junctions in relation to the position of the cardiac cells (Figure 3E). We observed that the expression of Cx43 does not present a specific pattern within the cardiac organoids, and it follows the arbitrary arrangement of the cells. Additionally, based on qualitative evaluation, there is no significant difference in the expression levels of Cx43 between experimental groups (Figure 3E, bottom). This was further confirmed by gene expression analysis of the GJA1 gene (Figure 4A). Overall, we demonstrated the formation to cell−cell adhesions through SAA and Cx43 costaining, confirming our hypothesis for the aggregation and interaction of the cardiac cells.

*2.2.4. Transcriptional Profile of the Cardiac Organoids.* The evaluation of the effects of coculture conditions and nutrient starvation at the transcriptional level was performed through qRT-PCR. We selected a panel of 12 genes relevant for cardiac structure (ACTN2, GJA1, MYH6, MYH7, TNNT2, TNNI3, MLC2V, and MLC2A) and genes involved in electrophysiological function and calcium ($Ca^{2+}$) handling (RYR2, SERCA, CASQ2, and S100A1). The cardiac organoids were harvested on day 7 after seeding and dissociated to extract the total mRNA. In order to include the effects of the nutrient deprivation in the hiPSC-CMs, the gene expression was normalized to a 2D cellular population on the day when the nutrient deprivation was started (D-1). Additionally, each group was matched to a D-1 control with similar cellular composition (i.e., monoculture and coculture conditions). We found that the B27C and SFC conditions presented a higher expression of most of these genes when compared to their monoculture counterpart (Figure 4A). Specifically, we found statistically significant higher expression of MYH7, MLC2A, and MLC2V (only for SFC).

Even when the expression was significantly higher for coculture groups, when compared to the gene expression levels of D-1, there was an overall downregulation of most of CMs structural genes, for example, GJA1 and MYH7 (Figure 4A, first and second columns). The downregulation of some these genes when the hiPSC-CMs are exposed to a 3D microenvironment have also been reported previously such as GJA1, MYH6, and MYH7.[53] For example, GJA1 is the gene in charge for the transcription of Cx43, and as previously discussed, organized localization and translocation of Cx43 to the cell membrane allows for the formation of a 3D syncytium that allows for electrical signal propagation.[54] The downregulation of this and other genes in cardiac organoids has been attributed to the simplicity of monoculture and coculture models as well as to a transcriptomic shift related to the 3D microenvironment and the relative immaturity of the hiPSC-derived cells.[55]

On the other hand, the majority of $Ca^{2+}$-handling genes, such as RYR2, SERCA, and S100A1, were upregulated for all experimental conditions, with no significant differences among the groups (Figure 4A, third column). This may be an indication that a 3D microenvironment is sufficient for promoting an enhanced electrophysiological phenotype of the hiPSC-CMs. Additionally, upregulation of RYR2 has been correlated to more mature hiPSC-CMs.[56]

The relative expression of each gene, compared to the other experimental groups was further evaluated through the calculation of the row Z-score (Figure 4B). We found that coculture groups (B27C and SFC) presented a relatively higher expression of the cardiac-relevant genes. This is a consequence of several factors. On one hand, the combination of 3D microenvironment and the coculture with hiPSC-CFs has been demonstrated to promote ECM organization,[55] providing mechanical support and anchorage for the hiPSC-CMs. This mechanical support serves several purposes, for instance, cell-to-ECM interactions and adhesion points can provide positive feedback to the intracellular structure of the hiPSC-CMs[57] and therefore inducing improved sarcomeric machinery. Additionally, the secretion of growth factors and other chemical cues, along with the cell-to-cell coupling, promotes improved intercellular interactions, inducing enhanced maturation of the hiPSC-CMs through paracrine signaling and crosstalk.[55] These findings are aligned with the rapid cardiac organoid compaction for our coculture experimental conditions, which we described during the morphological characterization of our ECTs.

The presented qRT-PCR analyses enabled us to assess some of the key gene regulation as a function of supplement starvation and coculture groups. Although, to broaden the gene expression evaluation utilizing a more modern and comprehensive method, such as RNA-seq may be required in future work. With this we expect to evaluate not only the structural conformation of the cardiac organoids, but also address other aspects of these ECTs, such as metabolic shifting and a closer assessment of the crosstalk between different cardiac cells.

*2.2.5. Electrophysiological Characterization of the Cardiac Organoids.* The electrophysiological characterization of ECTs is paramount in increasing utility of cardiac organoids in a myriad of applications.[58] For example, the ability to recapitulate the action potentials of the native heart *in vitro* can facilitate the evaluation of the proarrhythmic effect of drugs and small molecules, resulting in better *in vitro* systems for disease modeling and drug screening.[59,60] When


https://doi.org/10.1021/acsbiomaterials.2c01290
ACS Biomater. Sci. Eng. XXXX, XXX, XXX−XXX

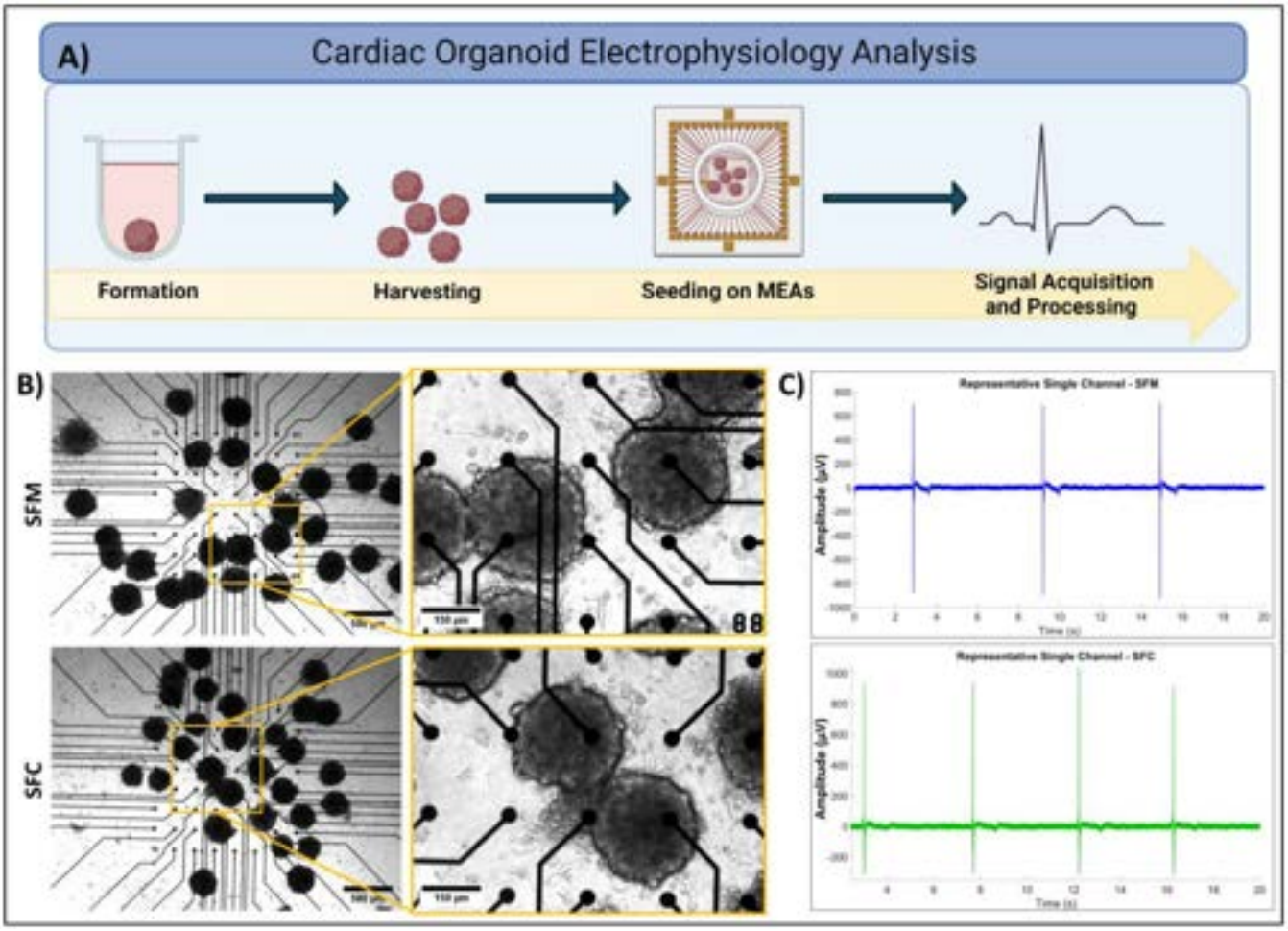


**Figure 5.** Electrophysiological characterization of cardiac organoids using MEAs. (A) Schematic representation of the methodology for the acquisition of the FPs from the cardiac organoids harvested on day 7 after seeding (created with Biorender.com). (B) Representative phase-contrast images of cardiac organoids seeded on MEAs (left, 2.5×; right, 10×; scale bars: 500 and 150 $\mu$m, respectively). (C) Representative FPs acquired from the cardiac organoids.

these models are created in combination with patient derived-hiPSCs, they can lead to personalized diagnosis and treatments.[58] Furthermore, understanding the electrical properties of cardiac organoids can help elucidate the mechanisms for coupling and engraftment to native tissue for cardiac regeneration applications. However, the electrophysiological evaluation of 3D cardiac microtissues is not trivial due to their size and geometry. Here we have used an MEA platform for recording the extracellular field potentials (FPs) on the surface of the cardiac organoids. Evaluation of the electrophysiological characteristics of cardiac organoids under supplement starvation regimen has never been described before, to the best of our knowledge. Thus, the focus of the FPs evaluation is only on the SFM and SFC groups.

First, the cardiac organoids were harvested 7 days after seeding in the agarose microwells and placed on the MEA wells. The microtissues were left undisturbed for at least 24 h to allow for recovery. After this period the FPs from the spontaneous beating were recorded (Figure 5A). In order to promote cellular adhesions to the glass surface of the MEA and to guarantee contact of the organoids with the microelectrodes the surface of the MEAs were coated with Matrigel. The surface treatment provided adhesion points to the cells in the microtissues that prevented the cardiac organoids from remaining in suspension and promoted a good contact between the tissues and the microelectrodes.

We observed that 24 h after seeding on the MEAs, the cardiac organoids were attached to the surface and some cells started to spread from the microtissues (Figure 5B). Additionally, the cardiac organoids presented spontaneous beating after the recovery period (Videos S8 and S9). The FPs from this spontaneous beating was recorded with the Intan stimulation/recording controller (Figure S5A).

The recorded signals consisted of a total of 60 channels, corresponding to each of the MEAs recording electrodes and the reference electrode. The FPs were recorded for periods of 20 s and presented the typical waveform of cardiac FPs (Figure 5C, Figure S6 and Figure S7).[60] In order to facilitate the visualization of the FPs, and moreover, to correlate specific MEA channels to the positioning of the cardiac organoids, we created heatmaps that represent the spatial localization of each electrode. These heatmaps represent features of the FPs that are paramount for the electrophysiological characterization of ECTs; for example, the FPs peak-to-peak amplitude and maximum and minimum values for each channel.[60,61] By overlaying these heatmaps on phase-contrast images of the corresponding groups (Figure 6A), we were able to identify the areas that presented the higher electrophysiological activity, allowing us to select ROIs for further signal processing. Additionally, we integrated these heatmaps and the acquired FPs to create videos of each of our experimental samples (Figure 6B and Video S10 and S11, the videos are shown at 0.5× speed to help with the visualization of the spontaneous beating). With this we have created a powerful tool to provide information about the spatiotemporal electrophysiological activity of the cardiac organoids seeded on the MEAs platform, which can offer more information about the activity of individual organoids


https://doi.org/10.1021/acsbiomaterials.2c01290
ACS Biomater. Sci. Eng. XXXX, XXX, XXX−XXX

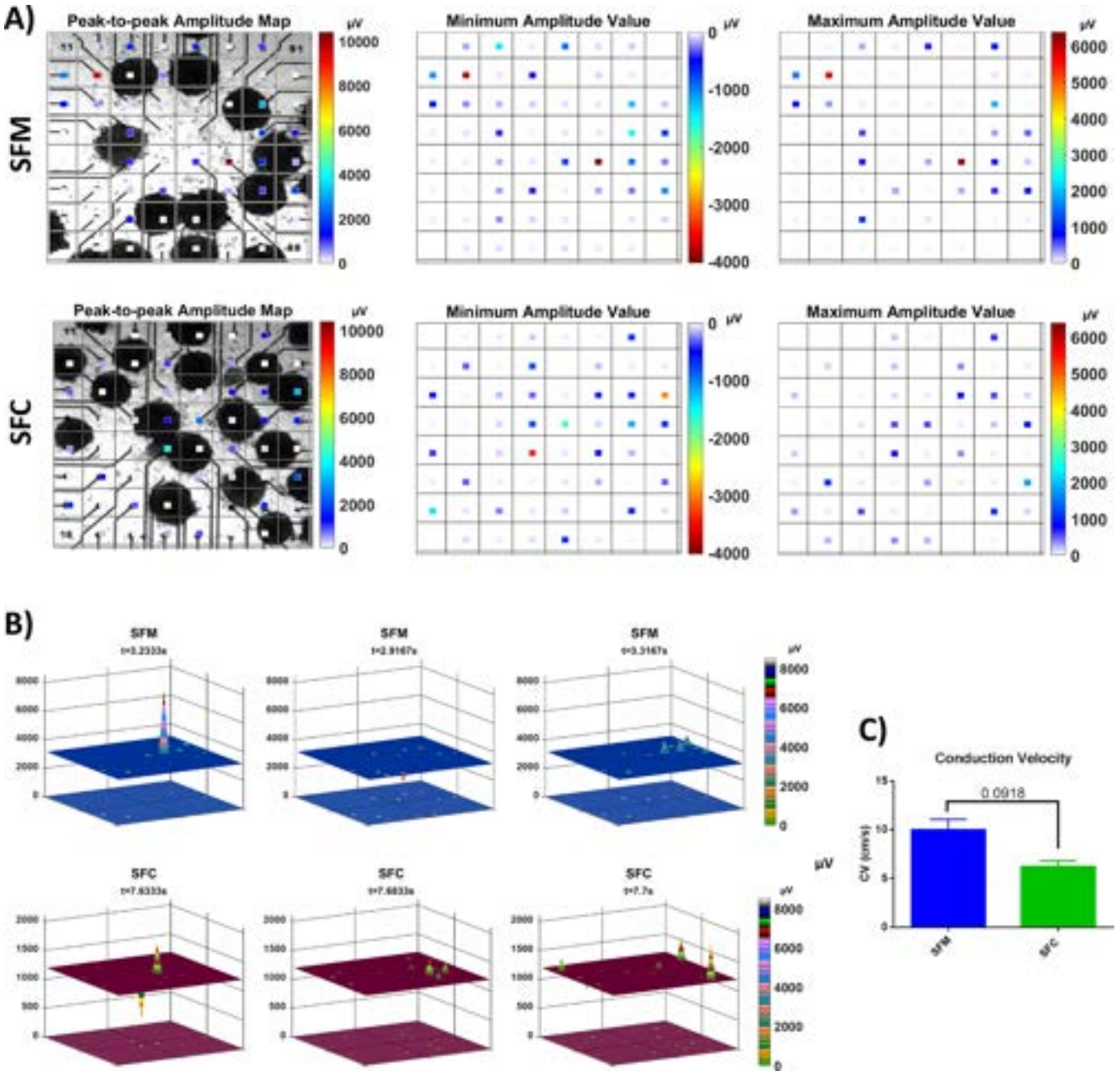


**Figure 6.** Evaluation of electrophysiological features of cardiac organoids from FPs. (A) Heatmaps of the peak-to-peak amplitude and maximum and minimum values of the FPs acquired with each individual channel of the MEA platform. The heatmaps were overlaid on phase-contrast images to show the localization of individual cardiac organoids. (B) Representative frames of the FPs amplitude videos generated from the acquired signals, extracted from Video S10 and Video S11, respectively. C) CV values for each of the analyzed experimental conditions. ($p$-value for significance: 0.05).

in relation with neighboring organoids and the overall tissue synchronicity.

The signals selected from ROIs were further processed in order to calculate the average CV for each experimental condition (Figure S8A and S8B). With this approach we proposed a straightforward method for calculating the CV of the cardiac organoids produced under supplement starvation regimen. We found CV values of 9.99 ± 1.07 cm/s and 6.20 ± 0.62 cm/s for the SFM and SFC organoids, respectively. Although the CV of the evaluated conditions was not significantly different ($p$ = 0.0918), we found a trend for a decreased signal propagation velocity in the SFC group (Figure 6C). This trend is in agreement with the rapid cellular aggregation and tissue compaction described earlier and is indicative of intercellular interactions between hiPSC-CMs and hiPSC-CFs. For example, it has been reported that CFs can electrically isolate the CMs in the tissue and obstruct the propagation of electrical signaling,[62] thus impeding a fast signal propagation and leading to a decreased CV. Also, it has been observed that this interference is dependent on the CFs density.[63]

Based on previous evidence, organoids enriched with hiPSC-CFs present a complex electromechanical behavior. On the one hand, CFs provide mechanical and chemical cues that are important for cellular survival and maturation.[55,57] Also, it has been reported that CFs present conductance and membrane potential different from those of the CMs, influencing in the overall electrical conduction of cardiac tissues.[64] In consequence, it was expected that our coculture experimental group showed a slower conduction velocity. These findings highlight the importance of an optimized coculture cellular


https://doi.org/10.1021/acsbiomaterials.2c01290
ACS Biomater. Sci. Eng. XXXX, XXX, XXX−XXX

ratio that can support the mechanical and chemical environment of the scaffold-free tissues but also do not hinder the desired electrophysiological properties of the organoids.[65] The extraction of other features from the acquired signals, such as waveform, and plateau time are subject of future work. This will lead to a better understanding and characterization of the electrical properties of the cardiac organoids.

## 3. CONCLUSION

In this study, we presented the formation of scaffold-free isogenic cardiac organoids derived from hiPSCs under a supplement starvation regimen. We demonstrated that the presence of hiPSC-CFs in the cardiac organoids significantly improved structural and physiological features of the cardiac organoids. This is reflected in enhanced gene expression of cardiac-relevant genes and improved morphology. These results are in alignment with the outcome of other isogenic and nonisogenic cardiac organoids reported in the literature.[20,31,66] In summary, there is a consensus that coculture cellular populations are beneficial to enhancing maturation and other features of the cardiac organoids.

Additionally, we found a trend for decreased CV that appears to be related to the presence of hiPSC-CFs, but this requires further investigation. We showed a modest improvement with the proposed supplement-free regimen, supporting the need of further optimization of the conditions of nutrient deprivation to improve the functionality of scaffold-free cardiac tissues. We confirmed that the inclusion of hiPSC-CFs in the cardiac organoids affects not only the morphology of the engineered tissues and their transcriptomic profile, but it also has an effect in the electrical behavior of the organoids. This trend is sufficient evidence to pursue a more thorough investigation regarding the features derived from the acquired FPs. Additionally, our approach demonstrates a straightforward method for a fast and simple evaluation of the basic electrophysiological characteristics of scaffold-free 3D cardiac organoids. The outcome of this study could be potentially utilized for the development of more physiologically relevant cardiac tissue models for disease modeling, drug testing, and regenerative medicine applications.[61,67,68]

## ■ ASSOCIATED CONTENT

### Supporting Information

The Supporting Information is available free of charge at https://pubs.acs.org/doi/10.1021/acsbiomaterials.2c01290.

Figure S1, immunostaining for hiPSCs (Nanog, Sox2) and hiPSC-CFs; Figure S2, phase-contrast images of hiPSC-CMs and cardiac organoids; Figure S3, TUNEL assay of sectioned cardiac organoids; Figure S4, sarcomere length quantification; Figure S5, electrophysiology equipment setup and diagram for CV calculation; Figure S6, SFM MEAs signal summary; Figure S7, SFC MEAs signal summary; Figure S8, calculation of conduction velocity using MEAs (PDF)

Video S1, hiPSC-CMs monolayer D-1 (before supplement starvation) (MP4)

Video S2, hiPSC-CMs monolayer D0 (supplemented media) (MP4)

Video S3, hiPSC-CMs monolayer D0 (supplement-free media) (MP4)

Video S4, B27M: representative cardiac organoid D7 (AVI)

Video S5, B27C: representative cardiac organoid D7 (AVI)

Video S6, SFM: representative cardiac organoid D7 (AVI)

Video S7, SFC: representative cardiac organoid D7 (AVI)

Video S8, SFM cardiac organoids seeded on MEAs (MP4)

Video S9, SFC cardiac organoids seeded on MEAs (MP4)

Video S10, SFM FPs amplitude heatmap (0.5× speed) (MP4)

Video S11, SFC FPs amplitude heatmap (0.5× speed) (MP4)

## ■ AUTHOR INFORMATION


### Corresponding Author

**Mehdi Nikkhah** − *School of Biological and Health Systems Engineering, Arizona State University, Tempe, Arizona 8528, United States; Center for Personalized Diagnostics Biodesign Institute, Arizona State University, Tempe, Arizona 85281, United States;* orcid.org/0000-0001-5970-7666; Email: mnikkhah@asu.edu

### Authors

**Alejandra Patino-Guerrero** − *School of Biological and Health Systems Engineering, Arizona State University, Tempe, Arizona 8528, United States;* orcid.org/0000-0003-1223-6558

**Ruben D. Ponce Wong** − *BMSEED, Mesa, Arizona 85201, United States*

**Vikram D. Kodibagkar** − *School of Biological and Health Systems Engineering, Arizona State University, Tempe, Arizona 8528, United States*

**Wuqiang Zhu** − *Department of Cardiovascular Diseases, Physiology and Biomedical Engineering, Mayo Clinic Arizona, Scottsdale, Arizona 85259, United States;* orcid.org/0000-0001-5217-7789

**Raymond Q. Migrino** − *Phoenix Veterans Affairs Health Care System, Phoenix, Arizona 85012, United States; University of Arizona College of Medicine, Phoenix, Arizona 85004, United States*

**Oliver Graudejus** − *BMSEED, Mesa, Arizona 85201, United States; School of Molecular Sciences, Arizona State University, Tempe, Arizona 85287, United States*

Complete contact information is available at: https://pubs.acs.org/10.1021/acsbiomaterials.2c01290


### Author Contributions

The manuscript was written through contributions of all authors. All authors have given approval to the final version of the manuscript.


### Funding

The authors acknowledge the Arizona Biomedical Research Commission (ABRC) New Investigator Award #AWD32676, the Flinn Foundation, and the National Science Foundation (NSF) CAREER Award #1653193 for providing funding sources for this project.


### Notes

The authors declare the following competing financial interest(s): A.P.G., V.D.K., W.Z., R.Q.M., and M.N. declare that they have no known competing financial interests or

personal relationships that could have appeared to influence the work reported in this paper. R.D.P.W. and O.G. are employed under Biomedical Sustainable Elastic Electronic Devices (BMSEED) LLC (BMSEED LLC).

## ■ ACKNOWLEDGMENTS

The authors thank Dr. Barbara Smith for providing access to qTower 2.0, and the Regenerative Medicine and Bioimaging Facility at Arizona State University for providing support with confocal imaging. Finally, we thank Dr. Jaimeson Veldhuizen and Hamid Esmaeili for providing support with hiPSC differentiation and cell sourcing.

## ■ REFERENCES

(1) Roth, G. A.; Mensah, G. A.; Johnson, C. O.; Addolorato, G.; Ammirati, E.; Baddour, L. M.; Barengo, N. C.; Beaton, A. Z.; Benjamin, E. J.; Benziger, C. P.; et al. Global Burden of Cardiovascular Diseases and Risk Factors, 1990−2019: Update From the GBD 2019 Study. *J. Am. Coll Cardiol* **2020**, *76* (25), 2982−3021.

(2) Yang, X.; Pabon, L.; Murry, C. E. Engineering adolescence: maturation of human pluripotent stem cell-derived cardiomyocytes. *Circ. Res.* **2014**, *114* (3), 511−523.

(3) Robertson, C.; Tran, D. D.; George, S. C. Concise review: maturation phases of human pluripotent stem cell-derived cardiomyocytes. *Stem Cells* **2013**, *31* (5), 829−837.

(4) Binah, O.; Dolnikov, K.; Sadan, O.; Shilkrut, M.; Zeevi-Levin, N.; Amit, M.; Danon, A.; Itskovitz-Eldor, J. Functional and developmental properties of human embryonic stem cells-derived cardiomyocytes. *J. Electrocardiol* **2007**, *40* (6), S192−S196.

(5) Snir, M.; Kehat, I.; Gepstein, A.; Coleman, R.; Itskovitz-Eldor, J.; Livne, E.; Gepstein, L. Assessment of the ultrastructural and proliferative properties of human embryonic stem cell-derived cardiomyocytes. *Am. J. Physiol Heart Circ Physiol* **2003**, *285* (6), H2355−2363.

(6) Veerman, C. C.; Kosmidis, G.; Mummery, C. L.; Casini, S.; Verkerk, A. O.; Bellin, M. Immaturity of human stem-cell-derived cardiomyocytes in culture: fatal flaw or soluble problem. *Stem Cells Dev* **2015**, *24* (9), 1035−1052.

(7) Veldhuizen, J.; Migrino, R. Q.; Nikkhah, M. Three-dimensional microengineered models of human cardiac diseases. *J. Biol. Eng.* **2019**, *13* (1), 29.

(8) Veldhuizen, J.; Cutts, J.; Brafman, D. A.; Migrino, R. Q.; Nikkhah, M. Engineering anisotropic human stem cell-derived three-dimensional cardiac tissue on-a-chip. *Biomaterials* **2020**, *256*, 120195.

(9) Navaei, A.; Saini, H.; Christenson, W.; Sullivan, R. T.; Ros, R.; Nikkhah, M. Gold nanorod-incorporated gelatin-based conductive hydrogels for engineering cardiac tissue constructs. *Acta Biomater* **2016**, *41*, 133−146.

(10) Navaei, A.; Moore, N.; Sullivan, R. T.; Truong, D.; Migrino, R. Q.; Nikkhah, M. Electrically conductive hydrogel-based micro-topographies for the development of organized cardiac tissues. *RSC Adv.* **2017**, *7* (6), 3302−3312.

(11) Esmaeili, H.; Patino-Guerrero, A.; Hasany, M.; Ansari, M. O.; Memic, A.; Dolatshahi-Pirouz, A.; Nikkhah, M. Electroconductive biomaterials for cardiac tissue engineering. *Acta Biomater* **2022**, *139*, 118−140.

(12) Gomez-Garcia, M. J.; Quesnel, E.; Al-Attar, R.; Laskary, A. R.; Laflamme, M. A. Maturation of human pluripotent stem cell derived cardiomyocytes in vitro and in vivo. *Semin Cell Dev Biol.* **2021**, *118*, 163−171.

(13) Navaei, A.; Rahmani Eliato, K.; Ros, R.; Migrino, R. Q.; Willis, B. C.; Nikkhah, M. The influence of electrically conductive and non-conductive nanocomposite scaffolds on the maturation and excitability of engineered cardiac tissues. *Biomater Sci.* **2019**, *7* (2), 585−595.

(14) Nikkhah, M.; Akbari, M.; Paul, A.; Memic, A.; Dolatshahi-Pirouz, A.; Khademhosseini, A. Gelatin-Based Biomaterials For Tissue Engineering And Stem Cell Bioengineering. *Biomaterials from Nature for Advanced Devices and Therapies* **2016**, 37−62.

(15) Woodcock, E. A.; Matkovich, S. J. Cardiomyocytes structure, function and associated pathologies. *Int. J. Biochem. Cell Biol.* **2005**, *37* (9), 1746−1751.

(16) Radisic, M.; Park, H.; Gerecht, S.; Cannizzaro, C.; Langer, R.; Vunjak-Novakovic, G. Biomimetic approach to cardiac tissue engineering. *Philos. Trans R Soc. Lond B Biol. Sci.* **2007**, *362* (1484), 1357−1368.

(17) Souders, C. A.; Bowers, S. L.; Baudino, T. A. Cardiac fibroblast: the renaissance cell. *Circ. Res.* **2009**, *105* (12), 1164−1176.

(18) Nugraha, B.; Buono, M. F.; Boehmer, L.; Hoerstrup, S. P.; Emmert, M. Y. Human Cardiac Organoids for Disease Modeling. *Clin Pharmacol Ther* **2019**, *105* (1), 79−85.

(19) Patino-Guerrero, A.; Veldhuizen, J.; Zhu, W.; Migrino, R. Q.; Nikkhah, M. Three-dimensional scaffold-free microtissues engineered for cardiac repair. *J. Mater. Chem. B* **2020**, *8* (34), 7571−7590.

(20) Beauchamp, P.; Jackson, C. B.; Ozhathil, L. C.; Agarkova, I.; Galindo, C. L.; Sawyer, D. B.; Suter, T. M.; Zuppinger, C.3D Co-culture of hiPSC-Derived Cardiomyocytes With Cardiac Fibroblasts Improves Tissue-Like Features of Cardiac Spheroids. *Frontiers in Molecular Biosciences***2020**, *7*, DOI: 10.3389/fmolb.2020.00014.

(21) Pinto, A. R.; Ilinykh, A.; Ivey, M. J.; Kuwabara, J. T.; D'Antoni, M. L.; Debuque, R.; Chandran, A.; Wang, L.; Arora, K.; Rosenthal, N. A.; et al. Revisiting Cardiac Cellular Composition. *Circ. Res.* **2016**, *118* (3), 400−409.

(22) Khammanit, R.; Chantakru, S.; Kitiyanant, Y.; Saikhun, J. Effect of serum starvation and chemical inhibitors on cell cycle synchronization of canine dermal fibroblasts. *Theriogenology* **2008**, *70* (1), 27−34.

(23) Fan, C.; Tang, Y.; Zhao, M.; Lou, X.; Pretorius, D.; Menasche, P.; Zhu, W.; Zhang, J. CHIR99021 and fibroblast growth factor 1 enhance the regenerative potency of human cardiac muscle patch after myocardial infarction in mice. *J. Mol. Cell Cardiol* **2020**, *141*, 1−10.

(24) Yang, J.; Ding, N.; Zhao, D.; Yu, Y.; Shao, C.; Ni, X.; Zhao, Z. A.; Li, Z.; Chen, J.; Ying, Z.; et al. Intermittent Starvation Promotes Maturation of Human Embryonic Stem Cell-Derived Cardiomyocytes. *Front Cell Dev Biol.* **2021**, *9*, 687769.

(25) Lian, X.; Zhang, J.; Azarin, S. M.; Zhu, K.; Hazeltine, L. B.; Bao, X.; Hsiao, C.; Kamp, T. J.; Palecek, S. P. Directed cardiomyocyte differentiation from human pluripotent stem cells by modulating Wnt/beta-catenin signaling under fully defined conditions. *Nat. Protoc* **2013**, *8* (1), 162−175.

(26) Zhang, J.; Tao, R.; Campbell, K. F.; Carvalho, J. L.; Ruiz, E. C.; Kim, G. C.; Schmuck, E. G.; Raval, A. N.; da Rocha, A. M.; Herron, T. J.; et al. Functional cardiac fibroblasts derived from human pluripotent stem cells via second heart field progenitors. *Nat. Commun.* **2019**, *10* (1), 2238.

(27) Kopanja, L.; Kralj, S.; Zunic, D.; Loncar, B.; Tadic, M. Core−shell superparamagnetic iron oxide nanoparticle (SPION) clusters: TEM micrograph analysis, particle design and shape analysis. *Ceram. Int.* **2016**, *42* (9), 10976−10984.

(28) Daghero, H.; Doffe, F.; Varela, B.; Yozzi, V.; Verdes, J. M.; Crispo, M.; Bollati-Fogolín, M.; Pagotto, R. Jejunum-derived NF-κB reporter organoids as 3D models for the study of TNF-alpha-induced inflammation. *Sci. Rep.* **2022**, *12* (1), 14425.

(29) Phelan, M. A.; Gianforcaro, A. L.; Gerstenhaber, J. A.; Lelkes, P. I. An Air Bubble-Isolating Rotating Wall Vessel Bioreactor for Improved Spheroid/Organoid Formation. *Tissue Engineering Part C: Methods* **2019**, *25* (8), 479−488.

(30) Khan, M. A.; Hashim, M. J.; Mustafa, H.; Baniyas, M. Y.; Al Suwaidi, S. K. B. M.; AlKatheeri, R.; Alblooshi, F. M. K.; Almatrooshi, M. E. A. H.; Alzaabi, M. E. H.; Al Darmaki, R. S.; Lootah, S. N. A. H. Global epidemiology of ischemic heart disease: results from the global burden of disease study. *Cureus* **2020**, *12* (7), e9349.

(31) Campostrini, G.; Meraviglia, V.; Giacomelli, E.; van Helden, R. W. J.; Yiangou, L.; Davis, R. P.; Bellin, M.; Orlova, V. V.; Mummery,



https://doi.org/10.1021/acsbiomaterials.2c01290
ACS Biomater. Sci. Eng. XXXX, XXX, XXX−XXX

C. L. Generation, functional analysis and applications of isogenic three-dimensional self-aggregating cardiac microtissues from human pluripotent stem cells. *Nat. Protoc* **2021**, *16* (4), 2213−2256.
(32) Tirziu, D.; Giordano, F. J.; Simons, M. Cell communications in the heart. *Circulation* **2010**, *122* (9), 928−937.
(33) Fan, D.; Takawale, A.; Lee, J.; Kassiri, Z. Cardiac fibroblasts, fibrosis and extracellular matrix remodeling in heart disease. *Fibrogenesis Tissue Repair* **2012**, *5* (1), 15.
(34) Doyle, M. J.; Lohr, J. L.; Chapman, C. S.; Koyano-Nakagawa, N.; Garry, M. G.; Garry, D. J. Human Induced Pluripotent Stem Cell-Derived Cardiomyocytes as a Model for Heart Development and Congenital Heart Disease. *Stem Cell Rev. Rep* **2015**, *11* (5), 710−727.
(35) Brewer, G. J.; Cotman, C. W. Survival and growth of hippocampal neurons in defined medium at low density: advantages of a sandwich culture technique or low oxygen. *Brain Res.* **1989**, *494* (1), 65−74.
(36) Brewer, G. J.; Torricelli, J. R.; Evege, E. K.; Price, P. J. Optimized survival of hippocampal neurons in B27-supplemented Neurobasal, a new serum-free medium combination. *J. Neurosci Res.* **1993**, *35* (5), 567−576.
(37) Correia, C.; Koshkin, A.; Duarte, P.; Hu, D.; Teixeira, A.; Domian, I.; Serra, M.; Alves, P. M. Distinct carbon sources affect structural and functional maturation of cardiomyocytes derived from human pluripotent stem cells. *Sci. Rep* **2017**, *7* (1), 8590.
(38) Ogasawara, T.; Okano, S.; Ichimura, H.; Kadota, S.; Tanaka, Y.; Minami, I.; Uesugi, M.; Wada, Y.; Saito, N.; Okada, K.; et al. Impact of extracellular matrix on engraftment and maturation of pluripotent stem cell-derived cardiomyocytes in a rat myocardial infarct model. *Sci. Rep* **2017**, *7* (1), 8630.
(39) Taddei, M.; Giannoni, E; Fiaschi, T; Chiarugi, P Global epidemiology of ischemic heart disease: results from the global burden of disease study. *J. Pathol.* **2012**, *226* (2), 380−393.
(40) Fennema, E.; Rivron, N.; Rouwkema, J.; van Blitterswijk, C.; de Boer, J. Spheroid culture as a tool for creating 3D complex tissues. *Trends Biotechnol.* **2013**, *31* (2), 108−115.
(41) Velasco, V.; Shariati, S. A.; Esfandyarpour, R. Microtechnology-based methods for organoid models. *Microsystems & Nanoengineering* **2020**, *6* (1), 76.
(42) Kang, S.-M.; Kim, D.; Lee, J.-H.; Takayama, S.; Park, J. Y. Engineered Microsystems for Spheroid and Organoid Studies. *Adv. Healthcaree Mater.* **2021**, *10* (2), 2001284.
(43) Roche, C. D.; Brereton, R. J. L.; Ashton, A. W.; Jackson, C.; Gentile, C. Current challenges in three-dimensional bioprinting heart tissues for cardiac surgery. *Eur. J. Cardiothorac Surg* **2020**, *58* (3), 500−510.
(44) Tan, Y.; Richards, D.; Coyle, R. C.; Yao, J.; Xu, R.; Gou, W.; Wang, H.; Menick, D. R.; Tian, B.; Mei, Y. Cell number per spheroid and electrical conductivity of nanowires influence the function of silicon nanowired human cardiac spheroids. *Acta Biomater* **2017**, *51*, 495−504.
(45) Radisic, M.; Deen, W.; Langer, R.; Vunjak-Novakovic, G. Mathematical model of oxygen distribution in engineered cardiac tissue with parallel channel array perfused with culture medium containing oxygen carriers. *Am. J. Physiol Heart Circ Physiol* **2005**, *288* (3), H1278−1289.
(46) Veldhuizen, J.; Chavan, R.; Moghadas, B.; Park, J. G.; Kodibagkar, V. D.; Migrino, R. Q.; Nikkhah, M. Cardiac ischemia on-a-chip to investigate cellular and molecular response of myocardial tissue under hypoxia. *Biomaterials* **2022**, *281*, 121336.
(47) Martin, T. G.; Kirk, J. A. Under construction: The dynamic assembly, maintenance, and degradation of the cardiac sarcomere. *J. Mol. Cell Cardiol* **2020**, *148*, 89−102.
(48) Sadayappan, S.; de Tombe, P. P. Cardiac myosin binding protein-C: redefining its structure and function. *Biophys Rev.* **2012**, *4* (2), 93−106.
(49) Pasqualini, F. S.; Sheehy, S. P.; Agarwal, A.; Aratyn-Schaus, Y.; Parker, K. K. Structural phenotyping of stem cell-derived cardiomyocytes. *Stem Cell Reports* **2015**, *4* (3), 340−347.
(50) Napiwocki, B. N.; Lang, D.; Stempien, A.; Zhang, J.; Vaidyanathan, R.; Makielski, J. C.; Eckhardt, L. L.; Glukhov, A. V.; Kamp, T. J.; Crone, W. C. Aligned human cardiac syncytium for in vitro analysis of electrical, structural, and mechanical readouts. B. *Biotechnol. Bioeng.* **2021**, *118* (1), 442−452.
(51) Nguyen, A. H.; Marsh, P.; Schmiess-Heine, L.; Burke, P. J.; Lee, A.; Lee, J.; Cao, H. Cardiac tissue engineering: state-of-the-art methods and outlook. *Journal of Biological Engineering* **2019**, *13* (1), 57.
(52) Carmeliet, E. Conduction in cardiac tissue. Historical reflections. *Physiological Reports* **2019**, *7* (1), e13860.
(53) Takada, T.; Sasaki, D.; Matsuura, K.; Miura, K.; Sakamoto, S.; Goto, H.; Ohya, T.; Iida, T.; Homma, J.; Shimizu, T.; et al. Aligned human induced pluripotent stem cell-derived cardiac tissue improves contractile properties through promoting unidirectional and synchronous cardiomyocyte contraction. *Biomaterials* **2022**, *281*, 121351.
(54) Biendarra-Tiegs, S. M.; Clemens, D. J.; Secreto, F. J.; Nelson, T. J. Human Induced Pluripotent Stem Cell-Derived Non-Cardiomyocytes Modulate Cardiac Electrophysiological Maturation Through Connexin 43-Mediated Cell-Cell Interactions. *Stem Cells Dev* **2020**, *29* (2), 75−89.
(55) Kerr, C. M.; Richards, D.; Menick, D. R.; Deleon-Pennell, K. Y.; Mei, Y. Multicellular Human Cardiac Organoids Transcriptomically Model Distinct Tissue-Level Features of Adult Myocardium. *Int. J. Mol. Sci.* **2021**, *22* (16), 8482.
(56) Jiang, Y.; Park, P.; Hong, S. M.; Ban, K. Maturation of Cardiomyocytes Derived from Human Pluripotent Stem Cells: Current Strategies and Limitations. *Mol. Cells* **2018**, *41* (7), 613−621.
(57) Valdoz, J. C.; Johnson, B. C.; Jacobs, D. J.; Franks, N. A.; Dodson, E. L.; Sanders, C.; Cribbs, C. G.; Van Ry, P. M. The ECM: To Scaffold, or Not to Scaffold, That Is the Question. *Int. J. Mol. Sci.* **2021**, *22* (23), 12690.
(58) Choi, J. S.; Lee, H. J.; Rajaraman, S.; Kim, D. H. Recent advances in three-dimensional microelectrode array technologies for in vitro and in vivo cardiac and neuronal interfaces. *Biosens Bioelectron* **2021**, *171*, 112687.
(59) Stella Stoter, A. M.; Hirt, M. N.; Stenzig, J.; Weinberger, F. Assessment of Cardiotoxicity With Stem Cell-based Strategies. *Clin Ther* **2020**, *42* (10), 1892−1910.
(60) Kussauer, S.; David, R.; Lemcke, H. hiPSCs Derived Cardiac Cells for Drug and Toxicity Screening and Disease Modeling: What Micro- Electrode-Array Analyses Can Tell Us. *Cells* **2019**, *8* (11), 1331.
(61) Kim, H.; Kamm, R. D.; Vunjak-Novakovic, G.; Wu, J. C. Progress in multicellular human cardiac organoids for clinical applications. *Cell Stem Cell* **2022**, *29* (4), 503−514.
(62) Vasquez, C.; Benamer, N.; Morley, G. E. The cardiac fibroblast: functional and electrophysiological considerations in healthy and diseased hearts. *J. Cardiovasc Pharmacol* **2011**, *57* (4), 380−388.
(63) Hall, C.; Gehmlich, K.; Denning, C.; Pavlovic, D. Complex Relationship Between Cardiac Fibroblasts and Cardiomyocytes in Health and Disease. *J. Am. Heart Assoc* **2021**, *10* (5), e019338.
(64) Bazhutina, A.; Balakina-Vikulova, N. A.; Kursanov, A.; Solovyova, O.; Panfilov, A.; Katsnelson, L. B. Mathematical modelling of the mechano-electric coupling in the human cardiomyocyte electrically connected with fibroblasts. *Prog. Biophys. Mol. Biol.* **2021**, *159*, 46−57.
(65) Saini, H.; Navaei, A.; Van Putten, A.; Nikkhah, M. 3D cardiac microtissues encapsulated with the co-culture of cardiomyocytes and cardiac fibroblasts. *Adv. Healthc Mater.* **2015**, *4* (13), 1961−1971.
(66) Beauchamp, P.; Moritz, W.; Kelm, J. M.; Ullrich, N. D.; Agarkova, I.; Anson, B. D.; Suter, T. M.; Zuppinger, C. Development and Characterization of a Scaffold-Free 3D Spheroid Model of Induced Pluripotent Stem Cell-Derived Human Cardiomyocytes. *Tissue Engineering Part C: Methods* **2015**, *21* (8), 852−861.
(67) Sakalem, M. E.; De Sibio, M. T.; da Costa, F. A. d. S.; de Oliveira, M. Historical evolution of spheroids and organoids, and possibilities of use in life sciences and medicine. *Biotechnology Journal* **2021**, *16* (5), 2000463.


https://doi.org/10.1021/acsbiomaterials.2c01290
ACS Biomater. Sci. Eng. XXXX, XXX, XXX−XXX

(68) Liu, Y.; Zhang, Y.; Mei, T.; Cao, H.; Hu, Y.; Jia, W.; Wang, J.; Zhang, Z.; Wang, Z.; Le, W.; Liu, Z. hESCs-Derived Early Vascular Cell Spheroids for Cardiac Tissue Vascular Engineering and Myocardial Infarction Treatment. *Advanced Science* **2022**, *9* (9), 2104299.



https://doi.org/10.1021/acsbiomaterials.2c01290
*ACS Biomater. Sci. Eng.* XXXX, XXX, XXX−XXX